# Interface Energetics and Charge Carrier Density Amplification by Sn-Doping in LaAlO$_3$/SrTiO$_3$ Heterostructure

Safdar Nazir, Jianli Cheng, Maziar Behtash, Jian Luo, and Kesong Yang*

Department of NanoEngineering, University of California, San Diego, 9500 Gilman Drive, Mail Code 0448, La Jolla, California 92093-0448, United States

**S** *Supporting Information*

**ABSTRACT:** Tailoring the two-dimensional electron gas (2DEG) at the *n*-type $(TiO_2)^0/(LaO)^{+1}$ interface between the polar LaAlO$_3$ (LAO) and nonpolar SrTiO$_3$ (STO) insulators can potentially provide desired functionalities for next-generation low-dimensional nanoelectronic devices. Here, we propose a new approach to tune the electronic and magnetic properties in the *n*-type LAO/STO heterostructure (HS) system via electron doping. In this work, we modeled four types of layer doped LAO/STO HS systems with Sn dopants at different cation sites and studied their electronic structures and interface energetics by using first-principles electronic structure calculations. We identified the thermodynamic stability conditions for each of the four proposed doped configurations with respect to the undoped LAO/STO interface. We further found that the Sn-doped LAO/STO HS system with Sn at Al site



(Sn@Al) is energetically most favorable with respect to decohesion, thereby strengthening the interface, while the doped HS system with Sn at La site (Sn@La) exhibits the lowest interfacial cohesion. Moreover, our results indicate that all the Sn-doped LAO/STO HS systems exhibit the *n*-type conductivity with the typical 2DEG characteristics except the Sn@La doped HS system, which shows *p*-type conductivity. In the Sn@Al doped HS model, the Sn dopant exists as a Sn$^{4+}$ ion and introduces one additional electron into the HS system, leading to a higher charge carrier density and larger magnetic moment than that of all the other doped HS systems. An enhanced charge confinement of the 2DEG along the *c*-axis is also found in the Sn@Al doped HS system. We hence suggest that Sn@Al doping can be an effective way to enhance the electrical conduction and magnetic moment of the 2DEG in LAO/STO HS systems in an energetically favorable manner.

**KEYWORDS:** 2DEG, perovskite oxide heterostructure, first-principles, doping, interface energetics, charge carrier density
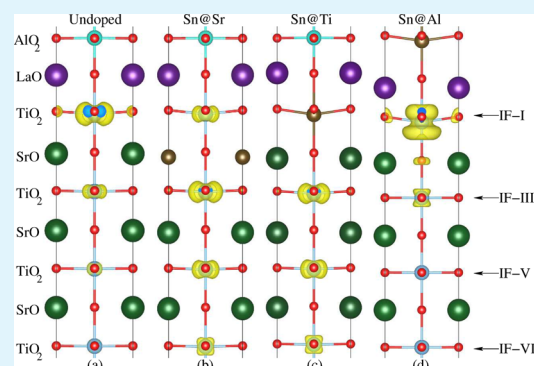
## 1. INTRODUCTION

Over the past decade, the formation of two-dimensional electron gas (2DEG) at the TiO$_2$-terminated *n*-type interfaces between the two insulators, nonpolar SrTiO$_3$ (STO) and polar LaAlO$_3$ (LAO), has stimulated extensive research interests because of its potential applications in the next-generation nanoelectronics.[1−9] The 2DEG occurring at the interface of the LAO/STO heterostructure (HS) is proposed to arise from the electronic reconstruction caused by the polar discontinuity between the polar (LaO)$^+$ and nonpolar (TiO$_2$)$^0$ layers.[10−12] Ideally, a net charge transfer of 0.5$e^-$ from the LAO film to the STO substrate per unit cell is required to compensate the polar discontinuity at the interface, forming interface metallic states by partially occupying Ti 3*d* orbitals,[10,13−15] which corresponds to a charge carrier density of about $3.2 \times 10^{14}$ cm$^{-2}$. Actually, the experimental charge carrier density is observed in the order of $10^{13}$ cm$^{-2}$, less than the ideal charge transfer of 0.5$e^-$/cell.[3,15,16] This can be attributed to several possible reasons such as the existence of the oxygen vacancies in the STO substrate,[17] and the polarization effects in the LAO film that partially counteract the polar discontinuity.[18]

Nevertheless, the 2DEG at perovskite oxide interfaces still has an exceptional electron transport property because of its high charge carrier density and mobility.[1,3,19] Besides this, the 2DEG on the LAO/STO interface also exhibits many other unique properties such as 2D Shubnikov-de Haas quantum oscillations,[20,21] ferromagnetism,[22−24] and coexistence of magnetism and superconductivity,[25,26] though the presence and nature of the intrinsic magnetism in the LAO/STO system is still under debate. On the one hand, there is no consistent conclusion on the observation of the magnetism from the experimental side. For example, Fitzsimmons et al. observed no magnetism in the LAO/STO superlattice via polarized neutron reflectometry measurements.[27] Salman et al. only found relatively small moments of $\sim 2 \times 10^{-3}$ $\mu_B$ per unit cell using β-detected nuclear magnetic resonance.[28] Kalisky et al. found that magnetism appears only above a critical LAO thickness below which magnetism is not observed, similar to the case of conductivity, using scanning superconducting quantum inter-

ference device microscopy.[29] On the other hand, theoretical work indicates that the 2DEG in the LAO/STO HS system may[30] or may not[31−33] produce intrinsic interface ferromagnetic order. Actually, the ferromagnetism is proposed to be induced by oxygen vacancies based on first-principles calculations.[32,33] Randeria et al.[34] even proposed that the evolution of the spiral state to ferromagnetic state in the external magnetic field is responsible for the experimental torque magnetometry data.[25] Despite the controversy of the mechanism on the interface magnetism, these unique properties provide great potential to enhance the functionality of the 2DEG-based nanoelectronic devices.

To maximize the functionality of the 2DEG in the LAO/STO system, a number of experimental[3−5,7,35−38] and theoretical[39−43] efforts have been made to tune its physical properties. There are several approaches such as defect engineering,[12,44−47] strain engineering,[7,35,39−41] and doping engineering, such as inserting new doping layers between the two perovskites,[42,48−56] to tailor the physical properties of the 2DEG in the perovskite oxide HS. For example, the oxygen vacancy in the LAO/STO HS was found to be able to dramatically tune the electron transport property[12,44,45] and enhance the magnetic moment,[46,57] while the Al vacancy was proposed to induce ferromagnetism in LAO/STO HS.[47]

In terms of the strain engineering, the tensile strain on the STO substrate was found to be able to enhance the interfacial conductivity and lateral charge confinement effects of the 2DEG in the LAO/STO.[7,35,39−41] Nevertheless, considering the practical difficulty of applying strain engineering on the STO substrate, inserting a new doping layer between the two perovskites appears to be more effective to tailor the properties of the 2DEG.[42,48−56] For instance, the transition metal and rare-earth metal doping at the STO side in the LAO/STO HS can significantly enhance the interfacial conductivity.[53,56] Insertion of one unit cell of $ATiO_3$ ($A$ = Ca, Sr, Sn, and Ba) at the interface and the rare-earth metal doping at the Sr site of the STO substrate can effectively modulate the sheet carrier density of the 2DEG in LAO/STO HS.[52] It was found that, compared with that of the undoped HS system, the La and Sn doping at the A site can lead to higher carrier density in the LAO/STO system. Hwang et al.[54] found that $LaTiO_3$-layer-doping can increase the charge carrier density of the LAO/STO HS, as predicted from first-principles calculations,[42] and the total charge carrier density reaches its maximum value at the doping of 0.5 unit cell of $LaTiO_3$. This is because extra electrons are introduced on the interface from the $Ti^{3+}$ ions of the $LaTiO_3$, and thus the interfacial charge carrier density is expected to continuously increase as more $LaTiO_3$ layers are introduced.[42] Nevertheless, it is experimentally observed that when more $LaTiO_3$ layers are introduced, the total charge carrier density of the LAO/STO HS decreases unexpectedly and slightly,[54] which is different from first-principles calculations.[42] This is probably because, in such a case, the $LaTiO_3$ layers far away from the STO substrate reserve more Mott insulating character, which is beyond the capability of standard density functional theory (DFT) calculation in describing the electronic states of Ti ions accurately, even within the frame of generalized gradient approximation (GGA) plus $U$ approach. Besides enhancing the electrical conductivity, the $\delta$-doping of $EuTiO_3$ layers between LAO and STO even leads to ferromagnetism.[55]

In a broader perspective, 2DEG is one exemplar showing that interfaces can exhibit properties that are drastically different from the corresponding bulk materials; such interfaces may be considered as 2D interfacial phases generally. Just like bulk phases, one effective way to tune the properties of 2D interfacial phases is to dope them with certain additives. Recent studies demonstrated that the formation of dopant- or defect-based 2D interfacial phases (also called complexions) can be utilized to tailor free surfaces,[58−60] grain boundaries,[61] and phase boundaries[62] either to achieve unique properties unattainable by conventional bulk materials or to control the materials fabrication processing. In this study, we explore a similar doping-based interfacial engineering strategy to tune the properties of LAO/STO interface by doping Sn at different atomic sites to form Sn-based stable or metastable 2D interfacial phases/complexions and to examine their stability conditions, that is, whether and at which conditions they may form and the impacts of their formation on 2DEG properties.

Specifically, to effectively tune the electron transport property of the 2DEG in the LAO/STO, one potential strategy is to introduce additional electrons into the polar LAO film via "electron doping". This can lead to more charge transfer from the LAO film to the nonpolar STO substrate, and thus the charge carrier density of the HS system can be significantly improved. Sn dopant often exists with an oxidation state of +4, and thus the substitutional Sn doping at $Al^{3+}$ site can introduce one more electron into the HS system, which can potentially increase the charge carrier density and thus enhance the electrical conductivity of the HS system. To verify this hypothesis, in this work, we modeled four substitutional Sn-doped LAO/STO HS structures, that is, Sn at Sr site (Sn@Sr), Sn at Ti site (Sn@Ti), Sn at La site (Sn@La), and Sn at Al site (Sn@Al), and studied their interfacial energetics, electronic, and magnetic properties using first-principles electronic structure calculations. We identified the thermodynamic stability conditions for each of the four proposed doped configurations with respect to the undoped LAO/STO interface, which can guide the search of the experimental conditions to growth such doped interfacial structures. We found that the Sn@Al doped LAO/STO HS system is energetically most favorable (with respect to decohesion) among the undoped and the other three doped HS systems (representing the highest mechanical stability), while the Sn@La doped HS system exhibits the lowest cohesion. As expected, the Sn@Al doping significantly amplifies the charge carrier density of the 2DEG and the magnetic moment of the interfacial Ti atoms compared with that of the undoped HS system. The electronic and magnetic properties of the other three Sn-doped LAO/STO HS systems are also detailed.

## 2. CALCULATION METHODS AND STRUCTURAL MODELING

Spin-polarized DFT calculations were performed using the Vienna Ab initio Simulation Package (VASP).[63,64] The projected augmented wave (PAW) potentials were used to treat the electron−ion interactions,[65] and the GGA parametrized by Perdew−Burke−Ernzerhof (PBE)[66] plus on-site Coulomb interaction approach (GGA+$U$) was used for the exchange−correlation functional along with $U$ = 5.8 and 7.5 eV for Ti 3$d$ and La 4$f$ orbitals, respectively. A cutoff of energy of 450 eV was used for the wave function expansion, and a $10 \times 10 \times 1$ $k$-space grid was found to converge well for the self-consistent calculations. Self-consistency was assumed for a total energy convergence of less than $10^{-5}$ eV. The density of states (DOS) was calculated with a Gaussian smearing of 0.05 eV. The initial magnetic moments of Ti ions in the spin-polarized DFT calculations were set in a ferromagnetic alignment. To resemble the experimental material growth process, all the atomic

positions and lattice parameters along the *z*-axis of the HSs are fully optimized until all components of the residual forces were smaller than 0.02 eV/Å, while the cell parameters along the *x*- and *y*-axis were fixed. The supercell approach was used to model the $(LAO)_{6.5}/(STO)_{11.5}$ HS, which contains two periodic *n*-type $(TiO_2)^0/(LaO)^{+1}$ symmetric interfaces. The experimental lattice constant of STO, 3.905 Å, was fixed in the *ab*-plane to construct all the HS systems. In this work, four Sn-cation-doped LAO/STO HS models were considered in which the Sn cation replaces the Sr (Sn@Sr), Ti (Sn@Ti), La (Sn@La), and Al (Sn@Al) atom near the interfacial region, respectively.

## 3. RESULTS AND DISCUSSION

### 3.1. Structural Relaxation and Interface Energetics.
The interfacial local structure reconstruction such as $TiO_6$ octahedron distortion strongly influences the interfacial electronic states of the LAO/STO HS.[18,67−69] To examine Sn doping effects on the interfacial structural deformation, we listed the optimized interfacial Ti−O (Sn−O and La−O) bond length along the *c*-axis and O−Ti−O (O−Sn−O) bond angles in Table 1. For comparison, the Ti−O (La−O) bond length

**Table 1. Calculated Interfacial Ti−O, Sn−O, and La−O Bond Lengths (Å) along the *c*-Axis (or *ac*-Plane) and O−Ti−O (O−Sn−O) Bond Angles in the *ab*-Plane for Undoped and Sn-Doped LAO/STO HS Systems**

| HS systems | Ti−O | Sn−O | O−Ti−O | O−Sn−O | La−O |
|---|---|---|---|---|---|
| undoped | 2.04 | | 172.4° | | 2.72 |
| Sn@Sr | 2.05 | | 168.5° | | 2.70 |
| Sn@Ti | | 2.16 | | 164.1° | 2.67 |
| Sn@La | 1.97 | 2.90 | 176.9° | | |
| Sn@Al | 2.30 | | 163.7° | | 2.49 |

and O−Ti−O bond angle of the undoped LAO/STO HS system are also listed. In all the doped and undoped systems, the interfacial $TiO_6$ or $SnO_6$ octahedra show structural distortion toward the STO substrate. In the Sn@Sr and Sn@Al doped systems, the interfacial Ti−O bond lengths increased by 0.01 and 0.26 Å, while the interfacial O−Ti−O bond angle decreased by 3.9° and 8.7°, respectively, with respect to that of the undoped LAO/STO system. This indicates that the interfacial $TiO_6$ octahedron becomes more distorted in the Sn@Al doped system than that in the undoped and Sn@Sr doped systems. As shown later, the structural distortion leads to a significant shrink of the La−O bond along the *ac*-plane and the resulting large cleavage energy and strong interfacial cohesion. In the Sn@La doped system, in contrast, the interfacial Ti−O bond distance decreases by 0.07 Å, while the O−Ti−O bond angle increases by 4.5° compared with that of the undoped LAO/STO system, which shows the opposite trend compared with the Sn@Sr and Sn@Al systems, implying that the interfacial $TiO_6$ octahedron is less distorted. Interestingly, the La−O bond length along the *ac*-plane in the Sn@Sr, Sn@Ti, and Sn@Al systems decreases by 0.02, 0.05, and 0.23 Å, respectively, with respect to that of the undoped system, suggesting that the interfacial La−O bond becomes stronger upon structural relaxation. In the Sn@La system, the Sn−O bond that corresponds to the La−O bond in the undoped system increases by 0.18 Å. As discussed below, the interfacial La−O bond length is correlated with the cleavage energies (interfacial cohesion) of the LAO/STO HS system.

To rigorously determine the relative thermodynamic stability of the undoped and various Sn-doped complexions, we need to know the relative interfacial energies, which depend on the

chemical potential of individual element, while the chemical potential strongly relies on the specific condition of materials synthesis. In other words, the relative thermodynamic stability of Sn-doped complexions is determined by the specific materials synthesis condition. The following equation compares the relative interfacial energies between the undoped and various Sn-doped LAO/STO HS complexions (interfacial structures):[70]

$$\gamma_{Sn@X} - \gamma_{undoped} = (E_{HS}^{Sn@X} - E_{HS}^{undoped} + 2\mu_X - 2\mu_{Sn})/2A \quad (1)$$

$\gamma_{Sn@X}$ (X = Sr, Ti, La, and Al) and $\gamma_{undoped}$ stand for the interfacial energies of the Sn-doped and undoped complexions, respectively. $E_{HS}^{Sn@X}$ and $E_{HS}^{undoped}$ are the total energies of the doped and undoped LAO/STO HS systems. $\mu_X$ (X = Sr, Ti, La, and Al) refers to the chemical potentials of the host ions, and $\mu_{Sn}$ is chemical potential of Sn. *A* is the interface area, and the factor of 2 in the denominator indicates that two symmetrical interfaces are present in the HS system. The factor of 2 of the chemical potentials $\mu_X$ and $\mu_{Sn}$ means two Sn atoms replacing two X atoms for constructing symmetrical interfaces. Note that the chemical potentials of the host ions and the Sn dopant depend on the materials growth conditions in the actual experiments. $\gamma_{Sn@X} - \gamma_{undoped} < 0$ suggests that the Sn@X doped HS system is energetically more favorable than the undoped HS system. Accordingly, $\mu_X - \mu_{Sn} < E_{HS}^{undoped} - E_{HS}^{Sn@X}$ suggests that the Sn@X (X = Sr, Ti, La, and Al) doped LAO/STO HS complexion (specific interfacial structure) is energetically (or thermodynamically) more favorable to form than the undoped system. Our calculations formulate this condition as the following four possibilities: (i) the Sn@Sr doped complexion is preferred to form with respect to the undoped LAO/STO interface when $\mu_{Sr} - \mu_{Sn} < 2.4$ eV; (ii) the Sn@Ti doped complexion is preferred when $\mu_{Ti} - \mu_{Sn} < 5.05$ eV; (iii) the Sn@La doped complexion is preferred when $\mu_{La} - \mu_{Sn} < 6.8$ eV; and (iv) the Sn@Al doped complexion is preferred when $\mu_{Al} - \mu_{Sn} < 6.25$ eV.

In addition, we calculated their cleavage energies ($E_{cleav}$) using the following formula:[70,71]

$$E_{cleav} = (E_{slab}^{STO} + E_{slab}^{LAO} - E_{HS})/2A \quad (2)$$

where $E_{HS}$ is the total energy of the LAO/STO HS system, while $E_{slab}^{STO}$ and $E_{slab}^{LAO}$ represent the total energy of the STO and LAO slab system, respectively. The STO and LAO slab systems are modeled using the same supercell with the HS system to maximize the error cancellation. As mentioned above, *A* refers to the interface area, and the factor of 2 in the denominator means the two symmetrical interfaces in the HS system. The physical meaning of the cleavage energy refers to the energy required to separate the HS system into two parts,[70] that is, the interfacial cohesion, which is independent of the specific chemical potentials of individual elements; therefore, $E_{cleav}$ can be robustly calculated with well-defined physical meaning (a measure of the mechanical stability or strength of the interface). As a result, the larger cleavage energy the HS system has, the stronger (generally more stable) interface. It is noted that the cleavage energy strongly depends on the interfacial bonding strength that can be partially reflected from the bond length. Herein, we plotted the interfacial La−O (Sn−O in Sn@La system) bond distance and cleavage energies of the undoped and Sn-doped LAO/STO HS systems in Figure 1, panels a and b, respectively. Our calculations show that the Sn@Sr, Sn@Ti,
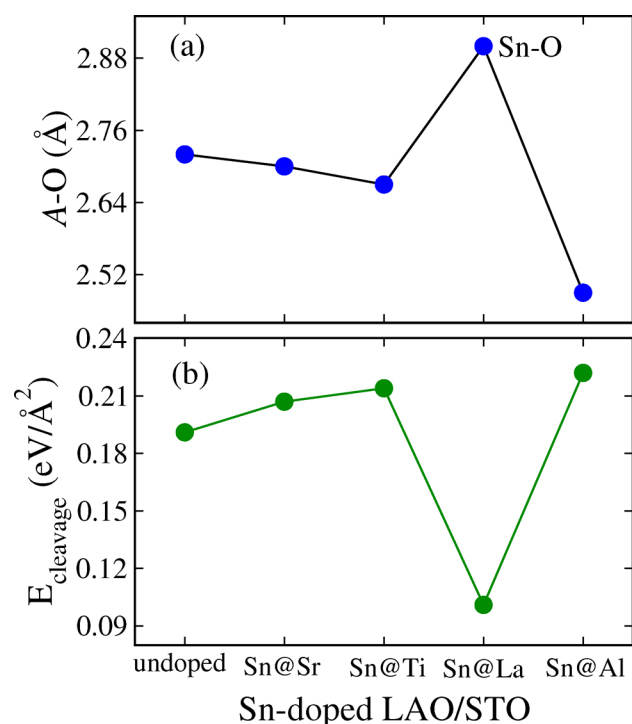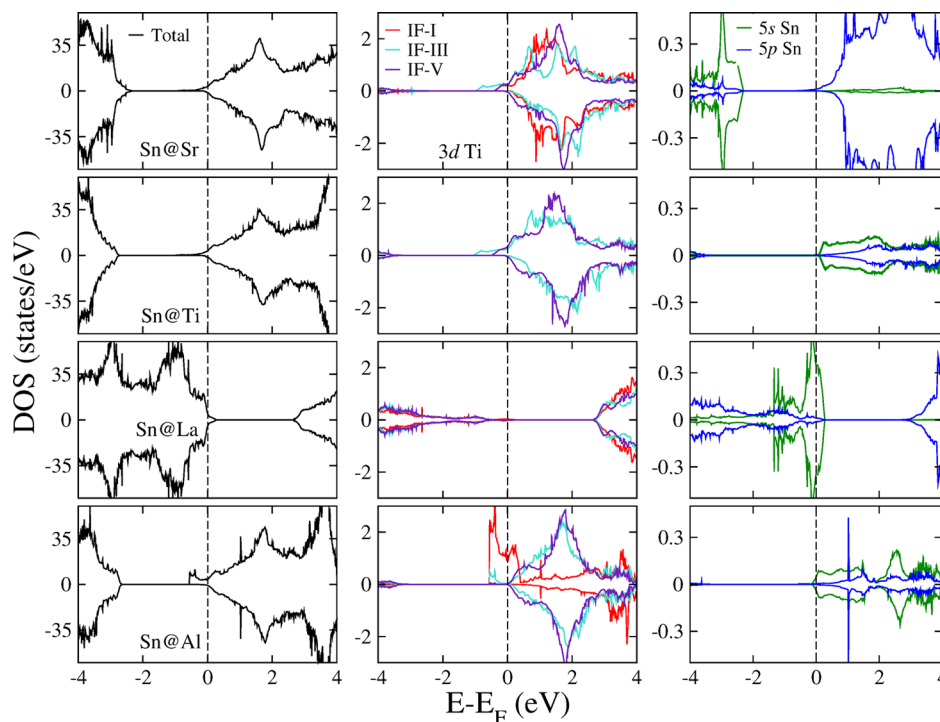
**Figure 1.** (a) Calculated A−O (A = La and Sn) bond distance along the *ac*-plane near the interfacial region and (b) cleavage energies as a function of undoped and Sn-doped LAO/STO HS systems. A−O bond refers to the La−O bond in the undoped, Sn@Sr, Sn@Ti, and Sn@Al doped LAO/STO systems, and Sn−O bond in the Sn@La doped system.

the undoped and various doped systems, implying that Sn@Al doping can stabilize significantly the LAO/STO HS system. This phenomenon can be understood from the changes of the interfacial chemical bond caused by the Sn doping, shown in Figure 1, panel a. Upon Sn doping, the interfacial La−O bond length is shortened in the Sn@Sr, Sn@Ti, and Sn@Al systems, which means the La−O bond strength increases. The Sn@Al doped system has the shortest La−O bond, that is, strongest interfacial bonding, and thus the highest cleavage energy. In contrast, in the Sn@La doped system, the Sn−O bond increases to 2.90 Å with respect to the corresponding La−O bond in the undoped LAO/STO HS system, which implies a weaker interfacial bonding and thus lower cleavage energy than the undoped and the other three Sn-doped HS systems. Hence, one would expect that Sn@La doping is energetically less favorable than the undoped and other three doped structures, and its preparation is relatively difficult. In short, our calculations indicate that the interfacial La−O bond length along the *ac*-plane could be used as effective descriptor for qualitatively evaluating the interfacial cohesion, and the substitutional Sn doping at Sr, Ti, and Al sites can enhance the La−O bonding strength.

**3.2. Electronic Properties.** In this section, we explored the electronic properties of various Sn-doped LAO/STO HS systems. The Sn-doping influence on the electronic states near the interfacial region was analyzed by plotting the total, partial Ti 3*d*, and Sn 5*s*/5*p* DOS for Sn@Sr, Sn@Ti, Sn@La, and Sn@Al doped LAO/STO HS systems, see Figure 2. It is well established that the 2DEG in the LAO/STO HS system is mainly caused by the partially occupied Ti 3*d* orbitals of the first interfacial (IF-I) $TiO_2$ layer of the STO substrate along with a small contribution from the third interfacial (IF-III) $TiO_2$ layer.[39−41] The fifth interfacial (IF-V) $TiO_2$ layer has almost negligible contribution, and the other layers away from

and Sn@Al doping strengthen the LAO/STO interfaces. The Sn@Al doping leads to the highest interfacial cohesion among



**Figure 2.** Calculated spin-polarized total and partial DOS projected on Ti 3*d* and Sn 5*s*/5*p* orbitals near the interfacial region of *n*-type (LaO)$^{+1}$/ (TiO$_2$)$^0$ interface for Sn@Sr (first row), Sn@Ti (second row), Sn@La (third row), and Sn@Al (fourth row) doped LAO/STO HS systems.

the interface have no contribution to the interfacial conductivity. The width of the conducting layers along the c-axis in the LAO/STO HS system is ~9.6 Å (about 3 unit cells of the STO), showing the two-dimensional characteristics of the 2DEG. Accordingly, we focused on the interfacial Ti 3d electronic states in the Sn-doped LAO/STO HS systems. The first, second, third, and fourth row in Figure 2 represent the Sn@Sr, Sn@Ti, Sn@La, and Sn@Al doped LAO/STO systems, respectively. To analyze the valence states of Sn ions, we also plotted partial DOS of Sn including its 5s and 5p orbitals for each system. The total DOS indicates that Sn@Sr, Sn@Ti, and Sn@Al doped LAO/STO systems exhibit n-type conductivity, while the Sn@La doped LAO/STO system shows p-type conductivity. As discussed below, the different conductivity types are caused by the different valence states of the Sn dopants.

For Sn@Sr doped LAO/STO system, it shows the nearly same total and partial DOS as found in the undoped LAO/STO HS, with a small decrease in the partial occupation of the DOS near the Fermi level, which will be reflected from the number of the orbital occupations in Figure 3. The partial DOS
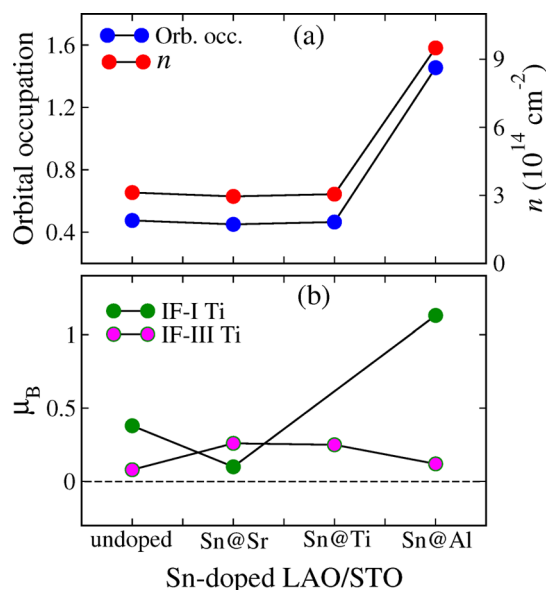


**Figure 3.** Calculated (a) total orbital occupation (Orb. occ.) numbers and corresponding charge carrier densities ($n$) and (b) partial Ti magnetic moments ($\mu_B$) near the interfacial (IF-I and IF-III) TiO$_2$ layers in the undoped and various Sn-doped LAO/STO HS systems.

of the Sn dopant illustrates that Sn 5s orbitals are fully occupied, while its 5p orbitals are fully empty. This means that Sn dopant has its electron configuration resembling that of a Sn$^{2+}$ ($s^2p^0$) ion, which shares the same valence state with that of the host Sr ion. Similarly, the Sn@Ti doped system also shows the nearly same total and partial DOS with that of the undoped LAO/STO HS system. The partial DOS plot of the Sn dopant shows that the majority of both Sn 5s and 5p orbitals are unoccupied, indicating that the Sn dopant has an electron configuration like that of a Sn$^{4+}$ ($s^0p^0$) ion, same with that of the host Ti$^{4+}$ ion. In both cases, the charge transferred from the polar (LaO)$^{+1}$ layer to the nonpolar (TiO$_2$)$^0$ layers toward the STO substrate. However, no additional electrons are introduced into the system, implying that Sn@Sr and Sn@Ti

doping is not an effective way to tune the conduction of the 2DEG in LAO/STO HS.

For Sn@La doped LAO/STO system, surprisingly, the Fermi level is pinned in the valence band tail, exhibiting p-type conductivity, see the third row in Figure 2. The partial DOS of the Sn shows that 5s orbitals slightly cross the Fermi level, while the majority of the 5p orbital is in the conduction band, indicating that the Sn approximately remains in the +2 state at the La site. That is to say, the Sn$^{2+}$ doping at the La$^{3+}$ site introduces one hole into the system, thus leading to the p-type conductivity. Our partial DOS analysis indicates that the hole states contributing to the p-type conductivity mainly come from the Sn 5s and O 2p orbitals in the SnO layer, along with a small contribution from O 2p orbitals in the interfacial TiO$_2$ layer, see Figure 1S of the Supporting Information. This mechanism, however, is different from the predicted but not observed yet p-type conductivity in SrO terminated (SrO)$^0$/(AlO$_2$)$^{-1}$ undoped LAO/STO HS system, in which the charge transfer from the (SrO)$^0$ layer to the (AlO$_2$)$^{-1}$ layer induced by the polar discontinuity plays a crucial role.[1]

The most striking result of the present study involves the Sn@Al doping near the interfacial region, where the electron transport property of the 2DEG is expected to be substantially enhanced as compared with all other Sn-doped systems, including the undoped LAO/STO HS, see the fourth row of Figure 2. The total and partial Ti 3d gap states at the IF-I layer shrink toward the conduction band but grow near the Fermi level, increasing their orbital occupation. As in the case of Sn@Ti doped LAO/STO system, the partial DOS of Sn shows that its 5s and 5p orbitals are both unoccupied, indicating that the Sn dopant exists as an Sn$^{4+}$ ion. As a result, by replacing the Al$^{3+}$ with Sn$^{4+}$, one extra electron is added into the system, which almost resides at the Ti site in the IF-I layer. This enhances the orbitals occupation and hence the charge carrier density. The partial DOS shows that the metallic states are mainly contributed by the Ti 3d states on the IF-I layer, and the Ti 3d orbital occupation is much higher than that in the undoped and other Sn-doped LAO/STO HS systems. This indicates that the electron transferred from the polar (LaO)$^{+1}$ layer to the nonpolar (TiO$_2$)$^0$ layer and introduced by Sn@Al doping mostly resides on the Ti ion in the IF-I layer.

**3.3. Charge Carrier Density and Magnetic Moment.** For a qualitative comparison of the various Sn-doped LAO/STO HS systems excluding Sn@La doped system, we computed their total charge carrier density and partial magnetic moments on the Ti atoms near the interfacial (IF-I and IF-III) TiO$_2$ layers for undoped, Sn@Sr, Sn@Ti, and Sn@Al doped systems. To do so, we calculated the partial occupation by integrating the total DOS of the occupied gap states near the Femi level and then proceeded to determine the charge carrier density in each system. The estimated occupation numbers and their corresponding charge carrier densities of the undoped and Sn-doped LAO/STO HS systems are shown in Figure 3, panel a. Our theoretical results affirm that the highest orbital occupation number and charge carrier density are obtained in the Sn@Al doped LAO/STO HS system. As discussed above, this phenomenon occurs because Sn replacement of Al donates one extra electron into the system, which extensively increases the orbital occupation number of the DOS near the Fermi energy and hence elevates the charge carrier density. In contrast, the Sn@Sr and Sn@Ti doped LAO/STO HS systems exhibit nearly the same orbital occupation number. This is because that Sn dopant shares the same valence state with the

host ions in the LAO/STO system, that is, $Sn^{2+}$ at $Sr^{2+}$ and $Sn^{4+}$ at $Ti^{4+}$, respectively.

Next, we addressed the Sn doping effects on the magnetic moments of the above-mentioned doped HS systems. It is well-known that the partially occupied Ti 3$d$ orbital mainly contribute to the magnetic moment of the $n$-type LAO/STO HS system.[39,72] Hence, herein we show the calculated local magnetic moment on the Ti atoms near the interfacial (IF-I and IF-III) TiO$_2$ layers for the undoped and Sn-doped LAO/STO HS systems in Figure 3, panel b. The Sn@Al doped LAO/STO system has the largest IF-I Ti magnetic moment compared with all other systems in the present study. This is because one more electron was introduced into the Sn@Al doped system, and the additional electron mostly resides on the Ti 3$d$ orbital in the IF-I layer, resulting in the larger magnetic moment. In contrast, the Ti atoms in the IF-III TiO$_2$ layers exhibit very weak spin-polarization with magnetic moments of 0.12 $\mu_B$. This is because fewer electrons are transferred to the IF-III layers as compared with the IF-I from the LaO layer. The layers away from the interface in the STO substrate show no spin-polarization. For Sn@Sr and Sn@Ti doped LAO/STO HS systems, the deeper TiO$_2$ layers in the STO substrate exhibit significant spin-polarization with magnetic moments of 0.26 $\mu_B$/0.09 $\mu_B$ and 0.25 $\mu_B$/0.12 $\mu_B$ in IF-III/IF-V layers, respectively.

This variance is because Sn@Sr and Sn@Ti doping considerably distort the TiO$_6$ octahedra in deeper layers of STO as compared with the undoped and Sn@Al doped systems (discussed later), which lead to stronger electrical polarization and thus facilate the charge migration to deeper TiO$_2$ layers in the STO substrate. In short, our results indicate that Sn@Al doped LAO/STO HS system is expected to show higher interfacial charge carrier density and more robust magnetic moment than the undoped and other Sn-doped LAO/STO HS systems. In addition, to elucidate the effect of $U$ value on the electronic property, interfacial charge carrier density, and magnetic moment on the interfacial Ti ions, we took the Sn@Al doped LAO/STO system as an example and recalculated its electronic structure within $U$ = 0 eV for Ti 3$d$ and $U$ = 7.5 eV for La 4$f$. The calculated total, partial Ti 3$d$, and Sn 5$s$/5$p$ DOS were provided in the Figure 2S of the Supporting Information. Our calculations show that Ti 3$d$ states from the IF-I TiO$_2$ layers are mainly contributing to the metallic states, and the 2DEG mostly resides in the interfacial TiO$_2$ layer in the STO substrate, as observed in the case when $U$ = 5.8 eV was applied on Ti 3$d$ orbitals. The calculated interfacial charge carrier density and magnetic moment on the interfacial Ti ions within the $U$ = 0 eV for Ti 3$d$ are 8.6 × 10$^{14}$ cm$^{-2}$ and 0.73 $\mu_B$, respectively, less than the corresponding values of 9.5 × 10$^{14}$ cm$^{-2}$ and 1.13 $\mu_B$ with $U$ = 5.8 eV for Ti 3$d$ orbital. Our results indicate that the $U$ value (5.8 eV) on the Ti 3$d$ orbital does not alter the electronic property dramatically, but improve the magnetic moment of interfacial Ti ions by about 55%.

### 3.4. Quantum Confinements of 2DEG along the c-Axis.

To examine Sn doping effects on the quantum confinement of electron gases along the $c$-axis, charge density plots projected on the occupied bands forming the 2DEG for undoped, Sn@Sr, Sn@Ti, and Sn@Al doped LAO/STO HS systems are shown in Figure 4, which give a direct visualization of the spatial extension of the 2DEG. In the undoped LAO/STO system, a majority of the transferred electrons from the LAO are localized in the first TiO$_2$ layer (IF-I) in the STO substrate, and the remaining electrons are transferred to the
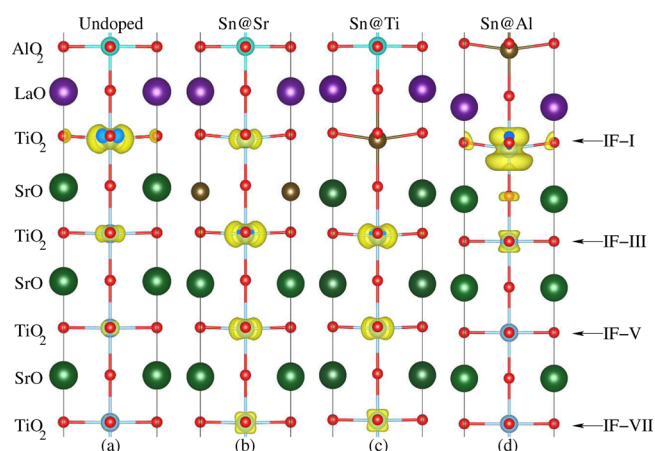


**Figure 4.** Charge density projected on the bands forming the metallic states near the interfacial region for (a) undoped, (b) Sn@Sr, (c) Sn@Ti, (d) and Sn@Al doped LAO/STO HS systems, respectively.

third (IF-III) and fifth (IF-V) layers of the STO substrate (Figure 4a). For the Sn@Al doped HS model, unexpectedly, the electrons transferred from the polar (LaO)$^{+1}$ layer to STO are almost completely confined in the first (TiO$_2$)$^0$ IF-I layer (Figure 4d), and only a very small amount of charge is transferred to the IF-III layer, forming a nearly ideal 2DEG. In the Sn@Sr doped HS system, besides the electrons localized on the IF-I TiO$_2$ layer, a substantial amount of electrons is transferred to the IF-III, IF-V, and IF-VII TiO$_2$ layers, extending the spatial thickness of the 2DEG substantially along the $c$-axis (Figure 4b). A similar phenomenon also occurs in Sn@Ti doped LAO/STO HS system. In this model, the interfacial SnO$_2$ (IF-1) layer cannot capture any electrons, and hence the electrons are further transferred to the IF-III, IF-V, and IF-VII TiO$_2$ layers. This indicates that the Sn@Sr and Sn@Ti doping weaken the quantum confinement effects of the 2DEG.

The extension of 2DEG is strongly related to the TiO$_6$ octahedra distortion in the STO substrate. To examine the degree of distortion, we calculated the angles of O−Ti−O in the $ab$-plane at the IF-III, IF-V, and IF-VII TiO$_2$ layers for undoped, Sn@Sr, Sn@Ti, and Sn@Al doped systems in Table 2. For the undoped system, one can clearly see that the TiO$_6$

**Table 2. Calculated O−Ti−O Bond Angles in the $ab$-Plane at IF-III, IF-V, and IF-VII TiO$_2$ Layers for Undoped, Sn@Sr, Sn@Ti, and Sn@Al Doped LAO/STO HS Systems**

|        | undoped | Sn@Sr  | Sn@Ti  | Sn@Al  |
|--------|---------|--------|--------|--------|
| IF-III | 177.6°  | 175.2° | 172.9° | 179.6° |
| IF-V   | 178.7°  | 176.3° | 176.1° | 179.8° |
| IF-VII | 179.3°  | 178.1° | 178.4° | 179.8° |

octahedra are distorted up to the third TiO$_2$ layer (IF-III), and therefore charge transfer from the LaO layer to the TiO$_2$ layer extends to three unit cells of the STO substrate, as indicated in the project charge density plot (Figure 4a). For the Sn@Al doped HS system, in contrast, very little TiO$_6$ octahedral distortion is found at the IF-III layer and is nearly absent at the IF-V/IF-VII TiO$_2$ layers. Therefore, less charge migrates to deeper layers, and a highly confined 2DEG is obtained. For Sn@Sr and Sn@Ti doped HS systems, the degree of TiO$_6$ distortion in deeper TiO$_2$ layers is much higher than that in the undoped and Sn@Al doped HS system. The TiO$_6$ distortion

toward the STO substrate results in an electric dipole moment, which further promotes the charge transfer to deep $TiO_2$ layers of the STO substrate and thus substantially extends the spatial thickness of 2DEG along the $c$-axis (see Figure 4b,c). It is worth mentioning that in the Sn@Al doped system, the shape of the charge density forming the 2DEG is vastly different from those in the undoped and other doped systems. To understand this phenomenon, we calculated the orbitally resolved Ti $3d$ DOS at the IF-I $TiO_2$ layer for undoped, Sn@Sr, and Sn@Al doped LAO/STO HS systems in Figure 5, panels a, b, and c,
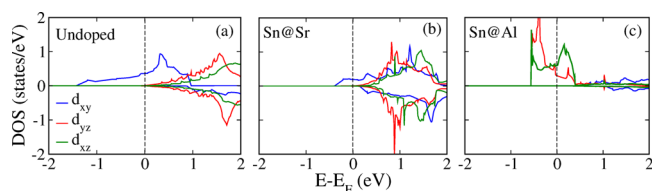


**Figure 5.** Calculated orbital-resolved Ti $3d$ DOS at the interfacial $TiO_2$ layers in (a) undoped, (b) Sn@Sr, (c) and Sn@Al doped LAO/STO HS systems.

respectively. For the undoped LAO/STO model, only $d_{xy}$ orbitals cross the Fermi level and are entirely responsible for the 2DEG, while the $d_{yz}$ and $d_{xz}$ orbitals remain unoccupied and do not contribute to interfacial conductivity, see Figure 5, panel a. A similar case also occurs in the Sn@Sr doped system, see Figure 5, panel b. For Sn@Al doped LAO/STO model, in contrast, the $d_{yz}$ and $d_{xz}$ orbitals contribute to the metallic states, while the $d_{xy}$ orbitals remain unoccupied and stay at higher energies in the conduction band, see Figure 5, panel c.

## 4. CONCLUSION

In conclusion, spin-polarized DFT calculations were performed to study the interfacial energetics, electronic, and magnetic properties of Sn-doped LAO/STO HS systems. Four substitutional Sn-doped LAO/STO HS structures, that is, Sn@Sr, Sn@Ti, Sn@La, and Sn@Al, are modeled. Our calculations identify the thermodynamic stability conditions of the four proposed doped structures with respect to the undoped LAO/STO HS and further show that Sn@Sr, Sn@Ti, and Sn@Al doping strengthens the LAO/STO interface by strengthening the La–O bonds, while the Sn@La doping weakens the interface. The relative interface cohesion of the four layer-doped LAO/STO systems (complexions) follows the order: Sn@Al > Sn@Ti > Sn@Sr > Sn@La. The Sn@Al, Sn@Ti, and Sn@Sr doped LAO/STO HS systems both show $n$-type conductivity with typical 2DEG characteristics, while the Sn@La doped HS system exhibits the $p$-type conductivity. The Sn@Al doped LAO/STO HS system is found to exhibit much higher charge carrier density and larger magnetic moment than those of the undoped, Sn@Sr, and Sn@Ti doped LAO/STO systems. This is because Sn@Al doping introduces one additional electron into the LAO/STO HS system, and the extra electron mostly resides in the $3d$ orbitals of interface Ti atoms. Thus, we propose that the electrical conduction and magnetic moment of the 2DEG in LAO/STO HS system can be amplified by Sn@Al doping in an energetically favorable way.

## ASSOCIATED CONTENT

**ⓈSupporting Information**
Calculated spin-polarized partial Sn $5s$ (at SnO layer) and O $2p$ (at SnO and IF-I $TiO_2$ layer) DOS for Sn@La doped LAO/ STO HS system; total, partial Ti $3d$, and Sn $5s/5p$ DOS with $U$ = 0 eV for Ti $3d$ orbital and $U$ = 7.5 eV for La $4f$ orbital. The Supporting Information is available free of charge on the ACS Publications website at DOI: 10.1021/acsami.5b02770.

## AUTHOR INFORMATION

**Corresponding Author**
*E-mail: kesong@ucsd.edu. Phone: +1-858-534-2514.
**Notes**
The authors declare no competing financial interest.

## REFERENCES

(1) Ohtomo, A.; Hwang, H. Y. A High-Mobility Electron Gas at the LaAlO$_3$/SrTiO$_3$ Heterointerface. *Nature* **2004**, *427*, 423−426.
(2) Okamoto, S.; Millis, A. J. Electronic Reconstruction at an Interface between a Mott Insulator and a Band Insulator. *Nature* **2004**, *428*, 630−633.
(3) Thiel, S.; Hammerl, G.; Schmehl, A.; Schneider, C. W.; Mannhart, J. Tunable Quasi-Two-Dimensional Electron Gases in Oxide Heterostructures. *Science* **2006**, *313*, 1942−1945.
(4) Cen, C.; Thiel, S.; Hammerl, G.; Schneider, C. W.; Andersen, K. E.; Hellberg, C. S.; Mannhart, J.; Levy, J. Nanoscale Control of an Interfacial Metal−Insulator Transition at Room Temperature. *Nat. Mater.* **2008**, *7*, 298−302.
(5) Cen, C.; Thiel, S.; Mannhart, J.; Levy, J. Oxide Nanoelectronics on Demand. *Science* **2009**, *323*, 1026−1030.
(6) Honig, M.; Sulpizio, J. A.; Joshua, J. D. A.; Zeldov, E.; Ilani, S. Local Electrostatic Imaging of Striped Domain Order in LaAlO$_3$/ SrTiO$_3$. *Nat. Mater.* **2013**, *12*, 1112−1118.
(7) Kalisky, B.; et al. Locally Enhanced Conductivity Due to the Tetragonal Domain Structure in LaAlO$_3$/SrTiO$_3$ Heterointerfaces. *Nat. Mater.* **2013**, *12*, 1091−1095.
(8) Sulpizio, J. A.; Ilani, S.; Irvin, P.; Levy, J. Nanoscale Phenomena in Oxide Heterostructures. *Annu. Rev. Mater. Sci.* **2014**, *44*, 117−149.
(9) Stemmer, S.; James Allen, S. Two-Dimensional Electron Gases at Complex Oxide Interfaces. *Annu. Rev. Mater. Sci.* **2014**, *44*, 151−171.
(10) Nakagawa, N.; Hwang, H. Y.; Muller, D. A. Why Some Interfaces Cannot Be Sharp. *Nat. Mater.* **2006**, *5*, 204−209.
(11) Savoia, A.; Paparo, D.; Perna, P.; Ristic, Z.; Salluzzo, M.; Miletto, G. F.; Scotti di Uccio, U.; Richter, C.; Thiel, S.; Mannhart, J.; Marrucci, L. Polar Catastrophe and Electronic Reconstructions at the LaAlO$_3$/SrTiO$_3$ Interface: Evidence from Optical Second Harmonic Generation. *Phys. Rev. B* **2009**, *80*, 075110.
(12) Liu, Z.; Li, C.; Lü, W.; Huang, X.; Huang, Z.; Zeng, S.; Qiu, X.; Huang, L.; Annadi, A.; Chen, J.; Coey, J.; Venkatesan, T.; Ariando. Origin of the Two-Dimensional Electron Gas at LaAlO$_3$/SrTiO$_3$ Interfaces: The Role of Oxygen Vacancies and Electronic Reconstruction. *Phys. Rev. X* **2013**, *3*, 021010.
(13) Son, W.-j.; Cho, E.; Lee, B.; Lee, J.; Han, S. Density and Spatial Distribution of Charge Carriers in the Intrinsic $n$-type LaAlO$_3$−SrTiO$_3$ Interface. *Phys. Rev. B* **2009**, *79*, 245411.
(14) Asmara, T. C.; Annadi, A.; Santoso, I.; Gogoi, P. K.; Kotlov, A.; Omer, H. M.; Motapothula, M.; Breese, M. B. H.; Rübhausen, M.; Venkatesan, T.; Ariando; Rusydi, A. Mechanisms of Charge Transfer and Redistribution in LaAlO$_3$/SrTiO$_3$ Revealed by High-Energy Optical Conductivity. *Nat. Commun.* **2014**, *5*, 3663.
(15) Cantoni, C.; Gazquez, J.; Granozio, F. M.; Oxley, M. P.; Varela, M.; Lupini, A. R.; Pennycook, S. J.; Aruta, C.; d. Uccio, U. S.; Perna, P.; Maccariello, D. Electron Transfer and Ionic Displacements at the Origin of the 2D Electron Gas at the LAO/STO Interface: Direct

Measurements with Atomic-Column Spatial Resolution. *Adv. Mater.* **2012**, *24*, 3952−3957.

(16) Liang, H.; Cheng, L.; Zhai, X.; Pan, N.; Guo, H.; Zhao, J.; Zhang, H.; Li, L.; Zhang, X.; Wang, X.; Zeng, C.; Zhang, Z.; Hou, J. G. Giant Photovoltaic Effects Driven by Residual Polar Field within Unit-Cell-Scale LaAlO₃ Films on SrTiO₃. *Sci. Rep.* **2013**, *3*, 1975.

(17) Siemons, W.; Koster, G.; Yamamoto, H.; Harrison, W. A.; Lucovsky, G.; Geballe, T. H.; Blank, D. H. A.; Beasley, M. R. Origin of Charge Density at LaAlO₃ on SrTiO₃ Heterointerfaces: Possibility of Intrinsic Doping. *Phys. Rev. Lett.* **2007**, *98*, 196802.

(18) Pentcheva, R.; Pickett, W. E. Avoiding the Polarization Catastrophe in LaAlO₃ Overlayers on SrTiO₃(001) through Polar Distortion. *Phys. Rev. Lett.* **2009**, *102*, 107602.

(19) Caviglia, A. D.; Gariglio, S.; Reyren, N.; Jaccard, D.; Schneider, T.; Gabay, M.; Thiel, S.; Hammerl, G.; Mannhart, J.; Triscone, J. M. Electric Field Control of the LaAlO₃/SrTiO₃ Interface Ground State. *Nature* **2008**, *456*, 624−627.

(20) Caviglia, A. D.; Gariglio, S.; Cancellieri, C.; Sacépé, B.; Fête, A.; Reyren, N.; Gabay, M.; Morpurgo, A. F.; Triscone, J.-M. Two-Dimensional Quantum Oscillations of the Conductance at LaAlO₃/SrTiO₃ Interfaces. *Phys. Rev. Lett.* **2010**, *105*, 236802.

(21) Fete, A.; Gariglio, S.; Berthod, C.; Li, D.; Stornaiuolo, D.; Gabay, M.; Triscone, J. M. Large Modulation of the Shubnikov-de Haas Oscillations by the Rashba Interaction at the LaAlO₃/SrTiO₃ Interface. *New J. Phys.* **2014**, *16*, 112002.

(22) Brinkman, A.; Huijben, M.; van Zalk, M.; Huijben, J.; Zeitler, U.; Maan, J. C.; van der Wiel, W. G.; Rijnders, G.; Blank, D. H. A.; Hilgenkamp, H. Magnetic Effects at the Interface between Non-magnetic Oxides. *Nat. Mater.* **2007**, *6*, 493−496.

(23) Ariando; Wang, X.; Baskaran, G.; Liu, Z. Q.; Huijben, J.; Yi, J. B.; Annadi, A.; Barman, A. R.; Rusydi, A.; Dhar, S.; Feng, Y. P.; Ding, J.; Hilgenkamp, H.; Venkatesan, T. Electronic Phase Separation at the LaAlO₃/SrTiO₃ Interface. *Nat. Commun.* **2010**, *2*, 188−194.

(24) Bi, F.; Huang, M.; Ryu, S.; B, C.-W.; Lee, H.; Eom, C.-B.; Irvin, P.; Levy, J. Room-Temperature Electronically-Controlled Ferromagnetism at the LaAlO₃/SrTiO₃ Interface. *Nat. Commun.* **2014**, *5*, 5019.

(25) Li, L.; Richter, C.; Mannhart, J.; Ashoori, R. C. Coexistence of Magnetic Order and Two-Dimensional Superconductivity at LaAlO₃/SrTiO₃ Interfaces. *Nat. Phys.* **2011**, *7*, 762−766.

(26) Bert, J. A.; Kalisky, B.; Bell, C.; Kim, M.; Hikita, Y.; Hwang, H. Y.; Moler, K. A. Direct Imaging of the Coexistence of Ferromagnetism and Superconductivity at the LaAlO₃/SrTiO₃ Interface. *Nat. Phys.* **2011**, *7*, 767−771.

(27) Fitzsimmons, M. R.; Hengartner, N. W.; Singh, S.; Zhernenkov, M.; Bruno, F. Y.; Santamaria, J.; Brinkman, A.; Huijben, M.; Molegraaf, H. J. A.; de la Venta, J.; Schuller, I. K. Upper Limit to Magnetism in LaAlO₃/SrTiO₃ Heterostructures. *Phys. Rev. Lett.* **2011**, *107*, 217201.

(28) Salman, Z.; Ofer, O.; Radovic, M.; Hao, H.; Shalom, B. M.; Chow, K. H.; Dagan, Y.; Hossain, M. D.; Levy, C. D. P.; MacFarlane, W. A.; Morris, G. M.; Patthey, L.; Pearson, M. R.; Saadaoui, H.; Schmitt, T.; Wang, D.; Kiefl, R. F. Nature of Weak Magnetism in SrTiO₃/LaAlO₃ Multilayers. *Phys. Rev. Lett.* **2012**, *109*, 257207.

(29) Kalisky, B.; Bert, J. A.; Klopfer, B. B.; Bell, C.; Sato, H. K.; Hosoda, M.; Hikita, Y.; Hwang, H. Y.; Moler, K. A. Critical Thickness for Ferromagnetism in LaAlO₃/SrTiO₃ Heterostructures. *Nat. Commun.* **2012**, *3*, 922.

(30) Pentcheva, R.; Pickett, W. E. Charge Localization or Itinerancy at LaAlO₃/SrTiO₃ Interfaces: Hole Polarons, Oxygen Vacancies, and Mobile Electrons. *Phys. Rev. B* **2006**, *74*, 035112.

(31) Chan, C. K.; Werner, P.; Millis, A. J. Magnetism and Orbital Ordering in an Interacting Three-Band Model: A Dynamical Mean-Field Study. *Phys. Rev. B* **2009**, *80*, 235114.

(32) Pavlenko, N.; Kopp, T.; Tsymbal, E. Y.; Mannhart, J.; Sawatzky, G. A. Oxygen Vacancies at Titanate Interfaces: Two-Dimensional Magnetism and Orbital Reconstruction. *Phys. Rev. B* **2012**, *86*, 064431.

(33) Pavlenko, N.; Kopp, T.; Tsymbal, E. Y.; Sawatzky, G. A.; Mannhart, J. Magnetic and Superconducting Phases at the LaAlO₃/SrTiO₃ Interface: The Role of Interfacial Ti 3*d* Electrons. *Phys. Rev. B* **2012**, *85*, 020407.

(34) Banerjee, S.; Erten, O.; Randeria, M. Ferromagnetic Exchange, Spin-Orbit Coupling, and Spiral Magnetism at the LaAlO₃/SrTiO₃ Interface. *Nat. Phys.* **2013**, *9*, 626−630.

(35) Bark, C. W.; Felker, D. A.; Wang, Y.; Zhang, Y.; Jang, H. W.; Folkman, C. M.; Park, J. W.; Baek, S. H.; Zhou, H.; Fong, D. D.; Pan, X. Q.; Tsymbal, E. Y.; Rzchowski, M. S.; Eom, C. B. Tailoring a Two-Dimensional Electron Gas at the LaAlO₃/SrTiO₃ (001) Interface by Epitaxial Strain. *Proc. Natl. Acad. Sci. U. S. A.* **2011**, *108*, 4720−4724.

(36) Mathew, S.; Annadi, A.; Chan, T. K.; Asmara, T. C.; Zhan, D.; Wang, X. R.; Azimi, S.; Shen, Z.; Rusydi, A.; Ariando; Breese, M. B. H.; Venkatesan, T. Tuning the Interface Conductivity of LaAlO₃/SrTiO₃ Using Ion Beams: Implications for Patterning. *ACS Nano* **2013**, *7*, 10572−10581.

(37) Irvin, P.; Ma, Y.; Bogorin, D. F.; Cen, C.; Bark, C. W.; Folkman, C. M.; Eom, C.-B.; Levy, J. Rewritable Nanoscale Oxide Photodetector. *Nat. Photonics* **2010**, *4*, 849−852.

(38) Tebano, A.; Fabbri, E.; Pergolesi, D.; Balestrino, G.; Traversa, E. Room-Temperature Giant Persistent Photoconductivity in SrTiO₃/LaAlO₃ Heterostructures. *ACS Nano* **2012**, *6*, 1278−1283.

(39) Nazir, S.; Behtash, M.; Yang, K. Enhancing Interfacial Conductivity and Spatial Charge Confinement of LaAlO₃/SrTiO₃ Heterostructures via Strain Engineering. *Appl. Phys. Lett.* **2014**, *105*, 141602.

(40) Nazir, S.; Yang, K. First-Principles Characterization of the Critical Thickness for Forming Metallic States in Strained LaAlO₃/SrTiO₃(001) Heterostructure. *ACS Appl. Mater. Interfaces* **2014**, *6*, 22351−22358.

(41) Nazir, S.; Behtash, M.; Yang, K. The Role of Uniaxial Strain in Tailoring the Interfacial Properties of LaAlO₃/SrTiO₃(001) Heterostructure. *RSC Adv.* **2015**, *5*, 15682−15689.

(42) Nazir, S.; Berna, C.; Yang, K. Modulated Two-Dimensional Charge Carrier Density in LaTiO₃-Layer-Doped LaAlO₃/SrTiO₃ Heterostructure. *ACS Appl. Mater. Interfaces* **2015**, *7*, 5305−5311.

(43) Nazir, S.; Behtash, M.; Yang, K. Towards Enhancing Two-Dimensional Electron Gas Quantum Confinement Effects in Perovskite Oxide Heterostructures. *J. Appl. Phys.* **2015**, *117*, 115305.

(44) Meevasana, W.; King, P. D. C.; He, R. H.; Mo, S.-K.; Hashimoto, M.; Tamai, A.; Songsiriritthigul, P.; Baumberger, F.; Shen, Z.-X. Creation and Control of a Two-Dimensional Electron Liquid at the Bare SrTiO₃ Surface. *Nat. Mater.* **2011**, *10*, 114−118.

(45) Yu, L.; Zunger, A. A Polarity-Induced Defect Mechanism for Conductivity and Magnetism at Polar−Nonpolar Oxide Interfaces. *Nat. Commun.* **2014**, *5*, 5118.

(46) Mohanta, N.; Taraphder, A. Oxygen vacancy clustering and pseudogap behaviour at the LaAlO₃/SrTiO₃ interface. *J. Phys.: Condens. Matter* **2014**, *26*, 215703.

(47) Weston, L.; Cui, X. Y.; Ringer, S. P.; Stampfl, C. Density-Functional Prediction of a Surface Magnetic Phase in SrTiO₃/LaAlO₃ Heterostructures Induced by Al Vacancies. *Phys. Rev. Lett.* **2014**, *113*, 186401.

(48) Fix, T.; MacManus-Driscoll, J. L.; Blamire, M. G. Delta-Doped LaAlO₃/SrTiO₃ Interfaces. *Appl. Phys. Lett.* **2009**, *94*, 172101.

(49) Fix, T.; Schoofs, F.; MacManus-Driscoll, J. L.; Blamire, M. G. Influence of Doping at the Nanoscale at LaAlO₃/SrTiO₃ Interfaces. *Appl. Phys. Lett.* **2010**, *97*, 072110.

(50) Choi, W. S.; Lee, S.; Cooper, V. R.; Lee, H. N. Fractionally δ-Doped Oxide Superlattices for Higher Carrier Mobilities. *Nano Lett.* **2012**, *12*, 4590−4594.

(51) Rastogi, A.; Pulikkotil, J. J.; Budhani, R. C. Enhanced Persistent Photoconductivity in δ-Doped LaAlO₃/SrTiO₃ Heterostructures. *Phys. Rev. B* **2014**, *89*, 125127.

(52) Frank, S.; Michael, A. C.; Mary, E. V.; Mehmet, E.; Thomas, F.; Josee, E. K.; McManus-Driscoll, J. L.; Mark, G. B. Carrier Density Modulation by Structural Distortions at Modified LaAlO₃/SrTiO₃ Interfaces. *J. Phys.: Condens. Matter* **2013**, *25*, 175005.

(53) Schoofs, F.; Egilmez, M.; Fix, T.; MacManus-Driscoll, J. L.; Blamire, M. G. Tuning the Two-Dimensional Carrier Density at LaAlO₃/SrTiO₃ Interfaces via Rare Earth Doping. *Solid State Commun.* **2013**, *156*, 35−37.

(54) Hosoda, M.; Bell, C.; Hikita, Y.; Hwang, H. Y. Compositional and Gate Tuning of the Interfacial Conductivity in $LaAlO_3/LaTiO_3/SrTiO_3$ Heterostructures. *Appl. Phys. Lett.* **2013**, *102*, 091601.

(55) De Luca, G. M.; Di Capua, R.; Di Gennaro, E.; Granozio, F. M.; Stornaiuolo, D.; Salluzzo, M.; Gadaleta, A.; Pallecchi, I.; Marrè, D.; Piamonteze, C.; Radovic, M.; Ristic, Z.; Rusponi, S. Transport Properties of a Quasi-Two-Dimensional Electron System Formed in $LaAlO_3/EuTiO_3/SrTiO_3$ Heterostructures. *Phys. Rev. B* **2014**, *89*, 224413.

(56) Disa, A. S.; Kumah, D. P.; Malashevich, A.; Chen, H.; Arena, D. A.; Specht, E. D.; Ismail-Beigi, S.; Walker, F. J.; Ahn, C. H. Orbital Engineering in Symmetry-Breaking Polar Heterostructures. *Phys. Rev. Lett.* **2015**, *114*, 026801.

(57) Salluzzo, M.; Gariglio, S.; Stornaiuolo, D.; Sessi, V.; Rusponi, S.; Piamonteze, C.; De Luca, G. M.; Minola, M.; Marré, D.; Gadaleta, A.; Brune, H.; Nolting, F.; Brookes, N. B.; Ghiringhelli, G. Origin of Interface Magnetism in $BiMnO_3/SrTiO_3$ and $LaAlO_3/SrTiO_3$ Heterostructures. *Phys. Rev. Lett.* **2013**, *111*, 087204.

(58) Kang, B.; Ceder, G. Battery Materials for Ultrafast Charging and Discharging. *Nature* **2009**, *458*, 190−193.

(59) Chen, X.; Liu, L.; Yu, P. Y.; Mao, S. S. Increasing Solar Absorption for Photocatalysis with Black Hydrogenated Titanium Dioxide Nanocrystals. *Science* **2011**, *331*, 746−750.

(60) Luo, J.; Chiang, Y.-M. Wetting and Prewetting on Ceramic Surfaces. *Annu. Rev. Mater. Res.* **2008**, *38*, 227−249.

(61) Cantwell, P. R.; Tang, M.; Dillon, S. J.; Luo, J.; Rohrer, G. S.; Harmer, M. P. Grain Boundary Complexions. *Acta Mater.* **2014**, *62*, 1−48.

(62) Baram, M.; Chatain, D.; Kaplan, W. D. Nanometer-Thick Equilibrium Films: The Interface between Thermodynamics and Atomistics. *Science* **2011**, *332*, 206−209.

(63) Kresse, G.; Furthmüller, J. Efficiency of Ab initio Total Energy Calculations for Metals and Semiconductors Using a Plane-Wave Basis Set. *Comput. Mater. Sci.* **1996**, *6*, 15−50.

(64) Kresse, G.; Furthmüller, J. Efficient Iterative Schemes for ab Initio Total-Energy Calculations Using a Plane-Wave Basis Set. *Phys. Rev. B* **1996**, *54*, 11169−11186.

(65) Blöchl, P. E. Projector Augmented-Wave Method. *Phys. Rev. B* **1994**, *50*, 17953−17979.

(66) Perdew, J. P.; Burke, K.; Ernzerhof, M. Generalized Gradient Approximation Made Simple. *Phys. Rev. Lett.* **1996**, *77*, 3865−3868.

(67) Okamoto, S.; Millis, A. J.; Spaldin, N. A. Lattice Relaxation in Oxide Heterostructures: $LaTiO_3/SrTiO_3$ Superlattices. *Phys. Rev. Lett.* **2006**, *97*, 056802.

(68) Hamann, D. R.; Muller, D. A.; Hwang, H. Y. Lattice-Polarization Effects on Electron-Gas Charge Densities in Ionic Superlattices. *Phys. Rev. B* **2006**, *73*, 195403.

(69) Pentcheva, R.; Pickett, W. E. Ionic Relaxation Contribution to the Electronic Reconstruction at the *n*-Type $LaAlO_3/SrTiO_3$ Interface. *Phys. Rev. B* **2008**, *78*, 205106.

(70) Dudiy, S. V.; Lundqvist, B. I. First-Principles Density-Functional Study of Metal−Carbonitride Interface Adhesion: Co/TiC(001) and Co/TiN(001). *Phys. Rev. B* **2001**, *64*, 045403.

(71) Hartford, J. Interface Energy and Electron Structure for Fe/VN. *Phys. Rev. B* **2000**, *61*, 2221−2229.

(72) Janicka, K.; Velev, J. P.; Tsymbal, E. Y. Magnetism of $LaAlO_3/SrTiO_3$ Superlattices. *J. Appl. Phys.* **2008**, *103*, 07B508.